

Landscape of pear-shaped even-even nuclei

Yuchen Cao (曹宇晨)^{1,2} S. E. Agbemava³ A. V. Afanasjev,³ W. Nazarewicz^{2,4,*} and E. Olsen⁵

¹*National Superconducting Cyclotron Laboratory, Michigan State University, East Lansing, Michigan 48824, USA*

²*Department of Physics and Astronomy, Michigan State University, East Lansing, Michigan 48824, USA*

³*Department of Physics and Astronomy, Mississippi State University, Starkville, Mississippi 39762, USA*

⁴*Facility for Rare Isotope Beams, Michigan State University, East Lansing, Michigan 48824, USA*

⁵*Institut d'Astronomie et d'Astrophysique, Université Libre de Bruxelles, 1050 Brussels, Belgium*



(Received 2 April 2020; accepted 27 July 2020; published 10 August 2020)

Background: The phenomenon of reflection-asymmetric nuclear shapes is relevant to nuclear stability, nuclear spectroscopy, nuclear decays and fission, and the search for new physics beyond the standard model. Global surveys of ground-state octupole deformation, performed with a limited number of models, suggest that the number of pear-shaped isotopes is fairly limited across the nuclear landscape.

Purpose: We carry out a global analysis of ground-state octupole deformations for particle-bound even-even nuclei with $Z \leq 110$ and $N \leq 210$ using nuclear density functional theory (DFT) with several nonrelativistic and covariant energy density functionals. In this way, we can identify the best candidates for reflection-asymmetric shapes.

Methods: The calculations are performed in the frameworks of axial reflection-asymmetric Hartree-Fock-Bogoliubov theory and relativistic Hartree-Bogoliubov theory using DFT solvers employing harmonic oscillator basis expansion. We consider five Skyrme and four covariant energy density functionals.

Results: We predict several regions of ground-state octupole deformation. In addition to the “traditional” regions of neutron-deficient actinide nuclei around ^{224}Ra and neutron-rich lanthanides around ^{146}Ba , we identified vast regions of reflection-asymmetric shapes in very neutron-rich nuclei around ^{200}Gd and ^{288}Pu , as well as in several nuclei around ^{112}Ba . Our analysis suggests several promising candidates with stable ground-state octupole deformation, primarily in the neutron-deficient actinide region, that can be reached experimentally. Detailed comparison between Skyrme and covariant models is performed.

Conclusions: Octupole shapes predicted in this study are consistent with the current experimental information. This work can serve as the starting point of a systematic search for parity doublets in odd-mass and odd-odd nuclei, which will be of interest in the context of new physics searches.

DOI: [10.1103/PhysRevC.102.024311](https://doi.org/10.1103/PhysRevC.102.024311)

I. INTRODUCTION

The majority of atomic nuclei have reflection-symmetric ground states (g.s.), and exhibit either spherical or ellipsoidal (prolate or oblate) shapes. In rare cases, however, the nucleus can spontaneously break its intrinsic reflection symmetry as a result of a nuclear Jahn-Teller effect [1–4] and acquire nonzero octupole moments associated with pearlike shapes [5–7] (see Refs. [8,9] for comprehensive reviews).

Early systematic calculations of octupole shapes were carried out with a macroscopic-microscopic approach based on the shell correction method [10–12] (see also Ref. [13] for an update). Those were followed by self-consistent studies within nuclear density functional theory (DFT) with Gogny [14–17], BCP [15,18], Skyrme [19,20], and covariant [21–24] energy density functionals.

Except for the global surveys [13,14,20,23,25], the majority of the previous DFT studies have focused on three specific regions of octupole collectivity: neutron-deficient actinides, neutron-rich lanthanides, and neutron-rich heavy and superheavy nuclei, which are important for the modeling of heavy-element nucleosynthesis. Consequently, to better understand systematic trends of octupole instability throughout the nuclear landscape, it is helpful to carry out additional global intermodel comparisons: that is the main objective of this work.

Additionally, the results of this study can provide robust candidates for atomic parity and time-reversal violation searches [26–28]. Of particular interest is the atomic electric dipole moment (EDM) [28]. The nuclear quantity behind the atomic EDM is the Schiff moment [29], which can be enhanced by the presence of nuclear octupole deformation [30–34]. In particular, a recent study [35] has demonstrated a correlation between the nuclear octupole deformation and the Schiff moment. Thus it is believed that the best candidates for atomic EDM measurements, such as ^{225}Ra , are nuclei with octupole shapes. A strong motivation for this work is

*witek@frib.msu.edu

to produce data for systematic Schiff moment calculations in odd-mass and odd-odd nuclei in the vicinity of the most robust octupole-deformed even-even candidates.

This paper is organized as follows. Section II describes the theoretical frameworks used. The results of our global calculations and an analysis of trends are presented in Sec. III. Local regions of octupole-deformed nuclei are discussed in Sec. IV. Finally, Sec. V contains a summary and conclusions.

II. THEORETICAL FRAMEWORK

Our calculations are performed in the framework of nuclear DFT [36]. They are restricted to axial shapes, as triaxiality affects the ground states of only a limited set of nuclei which do not overlap with regions of octupole deformation [13,20]. Moreover, the Skyrme DFT calculations in Ref. [20], which allow for nonaxial reflection asymmetric shapes, show that octupole-deformed lanthanides and actinides are axially symmetric.

A comment on our model selection is in order. To be useful in an analysis such as ours, a model must meet several stringent criteria. First, since it is meant to be used for extrapolations into unknown regions of the nuclear landscape, the selected model should be based on controlled many-body formalism employing quantified input (here, the energy density functional). Second, the underlying theoretical framework should be capable of reproducing basic nuclear properties (such as masses, radii, shell structure, and deformations). Finally, the model should be globally applicable throughout the nuclear chart. The models employed in this study are based on energy density functionals that were tested globally and that are consistent with bulk ground-state data. By using such validated models, we feel comfortable making predictions for new observables, such as octupole moments. The details pertaining to axial reflection-asymmetric Hartree-Fock-Bogoliubov (HFB) calculations (Sec. II A) and relativistic Hartree-Bogoliubov (RHB) calculations (Sec. II B) can be found in Refs. [37] and [23], respectively.

We studied particle-bound even-even nuclei with $Z \leq 110$ and $N \leq 210$. For nuclei with $Z \geq 112$, Coulomb frustration effects result in exotic topologies of nucleonic densities such as bubbles and tori [38–43], which give rise to instabilities of potential energy surfaces (PESs) due to configuration changes.

The axial shape deformations β_λ are defined through multipole moments $Q_{\lambda,0}$,

$$\begin{aligned}\beta_2 &= Q_{20} / \left(\sqrt{\frac{16\pi}{5}} \frac{3}{4\pi} AR_0^2 \right), \\ \beta_3 &= Q_{30} / \left(\sqrt{\frac{16\pi}{7}} \frac{3}{4\pi} AR_0^3 \right),\end{aligned}\quad (1)$$

where $R_0 = 1.2A^{1/3}$ and

$$\begin{aligned}Q_{20} &= \langle 2z^2 - x^2 - y^2 \rangle, \\ Q_{30} &= \langle z(2z^2 - 3x^2 - 3y^2) \rangle.\end{aligned}\quad (2)$$

Total/proton multipole moments are used in the HFB/RHB calculations, respectively. This difference is not critical since proton and neutron deformations are very similar in the range of nuclei considered. Note also that in the DFT calculations, all multipole moments (in our case, Q_{20} , Q_{30} , Q_{40} , Q_{50} , Q_{60}, \dots) that correspond to the energy minimum are obtained from the self-consistent particle density and the respective deformations (β_2 , β_3 , β_4 , β_5 , β_6, \dots) are computed from these moments. This is contrary to the macroscopic-microscopic approach in which the energy minimization is usually performed in a multidimensional space of selected deformations.

The magnitude of octupole deformation alone is insufficient to determine whether robust octupole deformation is present since it does not provide any information on the softness of the PES in the octupole direction. To address this issue, we also look at the gain in binding energy ΔE_{oct} due to octupole deformation:

$$\Delta E_{\text{oct}} = E^a(\beta_2, \beta_3) - E^s(\beta'_2, \beta'_3 = 0), \quad (3)$$

where E^a is the absolute binding energy obtained in reflection-asymmetric calculations, and E^s is the binding energy minimum from reflection-symmetric calculations. These two minima do not necessarily have the same quadrupole deformation. ΔE_{oct} is also an indicator of the stability of octupole-deformed shapes, where large values are typical for PESs with well-pronounced octupole minima; for such systems, the concept of static octupole deformation is better justified [8]. Conversely, small ΔE_{oct} values are characteristic of octupole-soft PESs typical of octupole vibrations; for such systems beyond-mean-field effects can play an important role [15,17,18,25,44–47].

A. Skyrme-Hartree-Fock-Bogoliubov calculations

In our study, we consider five Skyrme energy density functionals (SEDFs): UNEDF0 [48], UNEDF1 [49], UNEDF2 [50], SLy4 [51], and SV-min [52]. These SEDFs are described by means of 12–14 coupling constants. The root-mean-square error of the binding energy of these SEDFs, compared to the experimental mass data set AME2016 [53], ranges from 1.7 MeV (UNEDF0) to 5.3 MeV (SLy4). In the pairing channel, we took the mixed-type density-dependent delta interaction [54] with the Lipkin-Nogami approximate particle-number projection as in Ref. [55]. The pairing strengths for SLy4 and SV-min were assumed to be -258.2 and -214.28 MeV, respectively, assuming the same value for neutrons and protons.

The calculations were performed using the parallel DFT solver HFBTHO (v3.00) [56], which solves the HFB equation in the cylindrical deformed harmonic oscillator basis. We utilized the “kickoff” mode [56], whereby the multipole moments are constrained in the initial kickoff stage and subsequently released when certain criteria are met. Dynamic MPI scheduling was implemented to further reduce the computational cost of large-scale mass-table calculations.

The effectiveness and efficiency of the kickoff mode have been thoroughly tested and benchmarked with PES calculations of more than a hundred nuclei in various mass regions. A cylindrical harmonic oscillator basis of $N = 20$ major oscillator shells was used; this was tested to be equivalent

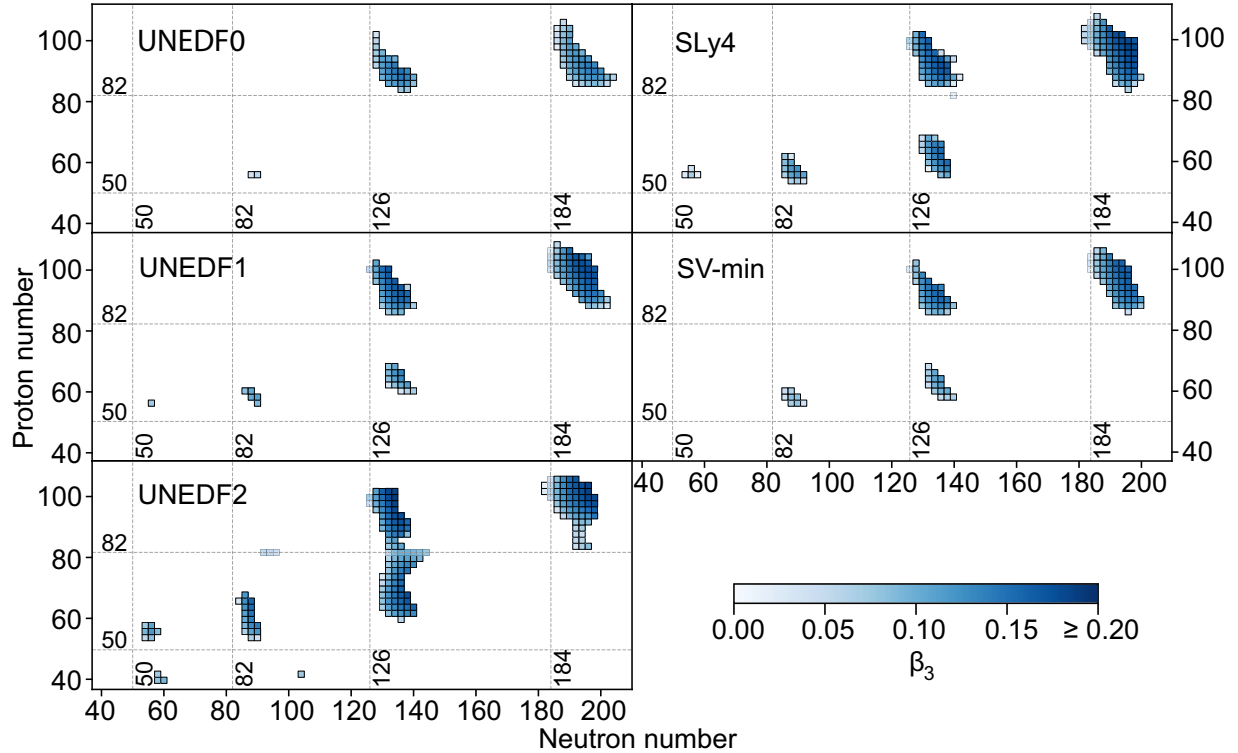


FIG. 1. Total g.s. octupole deformations β_3 of even-even nuclei in the (Z, N) plane predicted with the SEDFs UNEDF0, UNEDF1, UNEDF2, SLy4, and SV-min. Magic numbers are indicated by dashed lines.

(within a reasonable accuracy) in the prediction of g.s. masses compared to using larger shell numbers. Computational savings by using the kickoff mode and dynamic MPI scheduling, compared with PES calculations under static MPI scheduling, were found to be very significant.

B. Relativistic Hartree-Bogoliubov calculations

In the covariant DFT, the nucleus is considered to be a system of A nucleons which interact via the exchange of different mesons [57]. A global search for octupole-deformed nuclei has been performed using four covariant energy density functionals: DD-ME2 [58], NL3* [59], PC-PK1 [60], and DD-PC1 [61]. These CEDFs represent three major classes of covariant DFT models: the nonlinear meson-nucleon coupling model (represented by NL3*), the density-dependent meson exchange model (represented by DD-ME2), and the point coupling model (represented by DD-PC1 and PC-PK1). These functionals typically contain six to nine parameters which are fitted to experimental data on finite nuclei and nuclear matter properties [62]. We used separable pairing of finite range [63] with the strength defined as in Ref. [62]. Compared with the experimental AME2012 data set, the root-mean-square error of the binding energy of these CEDFs ranges from 2.15 MeV (DD-PC1) to 3.0 MeV (NL3*) [62].

The reflection-asymmetric RHB calculations are carried out using a parallel version of the computer code developed in Ref. [23], formulated in an axially deformed harmonic oscillator basis. In the present paper, additional calculations to those presented in Refs. [23,24] have been performed to cover the

same range of nuclei as in the Skyrme HFB calculations. The procedure, similar to the kickoff procedure employed in the HFBTHO calculations, is also used in the RHB calculations. However, in this case the set of initial Woods-Saxon pearlike densities defined by the basis deformations are used at the initial step of the calculations to push the convergence to the octupole-deformed minimum.

III. GLOBAL SURVEY

The g.s. octupole deformations β_3 obtained in our HFB calculations are displayed in Fig. 1. (For RHB results, see Refs. [23,24].) There is a good intermodel consistency, with large octupole deformations predicted around ^{146}Ba (neutron-rich lanthanides), ^{200}Gd (very neutron-rich lanthanides), ^{224}Ra (neutron-deficient actinides), and ^{288}Pu (neutron-rich actinides), i.e., in the regions of strong octupole collectivity defined by the presence of close-lying proton and neutron shells with $\Delta\ell = \Delta j = 3$ [8]. This finding is consistent with previous global studies [13,14,20,23,25].

In each region of octupole-deformed nuclei, the magnitude of octupole deformation increases with the number of valence nucleons. All five SEDFs predict neutron-deficient and neutron-rich actinides to exhibit strong octupole deformations, while predictions in the lanthanide region are less uniform regarding which nuclei are deformed and how deformed they are. In general, UNEDF2 and SLy4 predict the largest number of octupole-deformed nuclei and also the larger values of β_3 . In both models, proton-rich nuclei around ^{112}Ba are expected to be reflection asymmetric. The functional

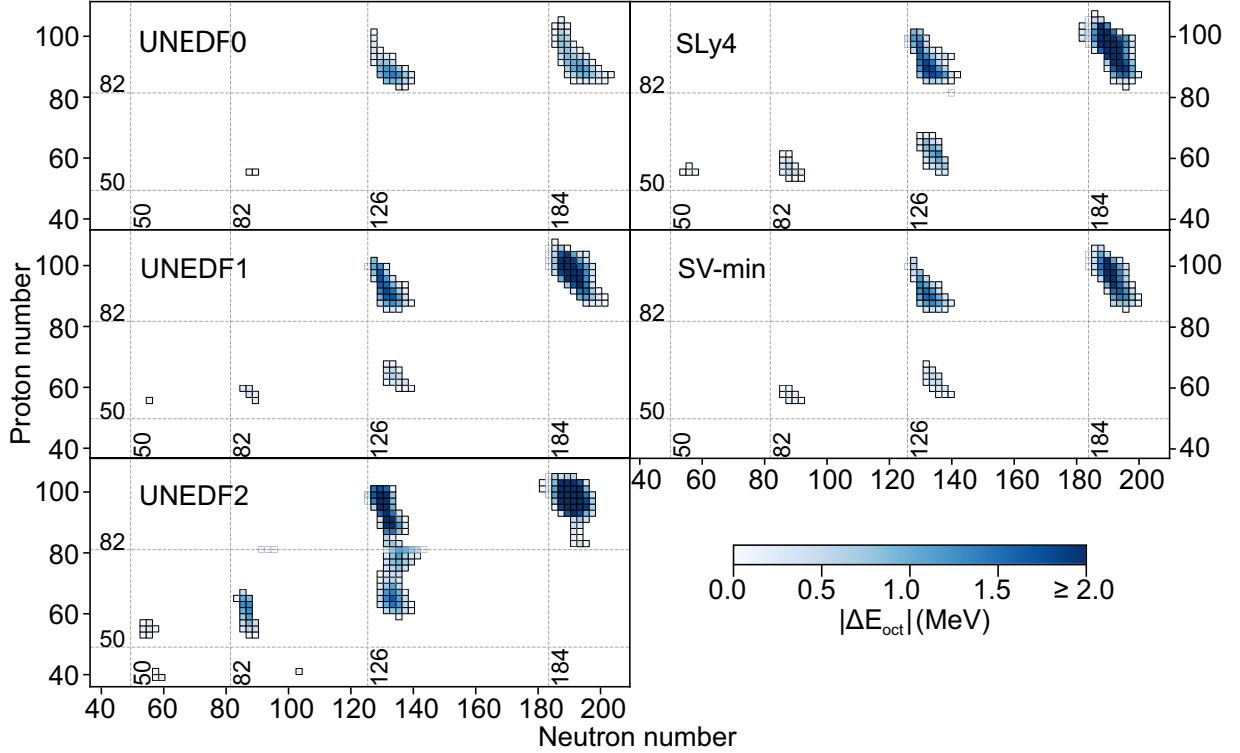


FIG. 2. Similar to Fig. 1, but for the octupole deformation energy ΔE_{oct} .

UNEDF0 predicts the lowest amount of octupole-deformed nuclei and smaller β_3 deformations overall.

The octupole deformation energies ΔE_{oct} predicted in our HFB calculations are shown in Fig. 2. (For RHB results, see Refs. [23,24].) We can see that lanthanide nuclei have appreciably smaller ΔE_{oct} values compared to the actinides in spite of similar octupole deformations. This indicates that most of the reflection-asymmetric lanthanide nuclei are predicted to have very soft PESs in the octupole direction, regardless of the equilibrium value of β_3 .

Microscopically, octupole deformations can be traced back to close-lying pairs of single-particle (s.p.) shells coupled by the octupole interaction [8]. Each pair consists of the unusual-parity intruder shell (ℓ, j) and the normal-parity shell ($\ell - 3, j - 3$). Consequently, the regions of nuclei with strong octupole correlations correspond to particle numbers near 34 ($g_{9/2} \leftrightarrow p_{3/2}$ coupling), 56 ($h_{11/2} \leftrightarrow d_{5/2}$), 88 ($i_{13/2} \leftrightarrow f_{7/2}$), 134 ($j_{15/2} \leftrightarrow g_{9/2}$), and 196 ($k_{17/2} \leftrightarrow h_{11/2}$).

Figure 3 shows the energy splitting

$$\Delta e = e(\ell, j) - e(\ell - 3, j - 3), \quad (4)$$

between s.p. canonical shells obtained from spherical HFB/RHB calculations. In general, there is a systematic decrease in Δe with mass, which—together with the increased degeneracy of s.p. orbits (and matrix elements of the octupole coupling)—results in enhanced octupole correlations in heavy nuclei. However, while this general trend is robust, the magnitude of Δe is not a good indicator of octupole correlations when comparing different models. Indeed, when comparing different models one also needs to consider other factors related to each model's structure. For instance, the

isoscalar effective mass of SLy4 is close to 0.7, which effectively increases the s.p. splitting compared to UNEDF models (which have an effective mass close to 1). As a result, although in most cases SLy4 has larger Δe than UNEDF1, it predicts more octupole-deformed nuclei and larger ΔE_{oct} values. When comparing predictions of the UNEDF family of SEDFs, the UNEDF2 parametrization constrained to the spin-orbit splittings in several nuclei yields the lowest values of Δe for neutrons and predicts the strongest octupole correlations (see Figs. 1 and 2). Still the relation between the size of Δe and the appearance of octupole deformations is very indirect: while the very appearance of $\Delta j = \Delta \ell = 3$ doublets with low $|\Delta e|$ creates favorable conditions for reflection-asymmetric shapes in a given region, this does not reveal anything about the magnitude of the symmetry breaking.

In an effort to obtain a more robust picture of octupole deformations, we combined the octupole predictions from the five SEDFs and four CEDFs in Fig. 4. We define the model multiplicity $m(Z, N) = k$ if a nucleus (Z, N) is predicted by k models ($k = 1, \dots, 9$) to have a nonzero octupole deformation. Nuclei predicted by all nine EDFs as octupole deformed (i.e., $m = 9$) are shown by stars. These are ^{146}Ba , $^{224,226}\text{Ra}$, $^{226,228}\text{Th}$, and ^{228}Pu in the regions experimentally accessible and in the very neutron-rich actinides: $^{288,290}\text{Pu}$, $^{288,290}\text{Cm}$, and $^{288,290}\text{Cf}$. The supplemental table [67] contains predicted values of ΔE_{oct} and β_3 values of nuclei with $m \geq 6$ as well as proton quadrupole and octupole moments in nuclei with $\beta_3 \geq 0.01$.

Apart from the overall agreement between SEDFs and CEDFs when it comes to the predicted regions of octupole instability, we see systematic shifts (by two to four neutrons)

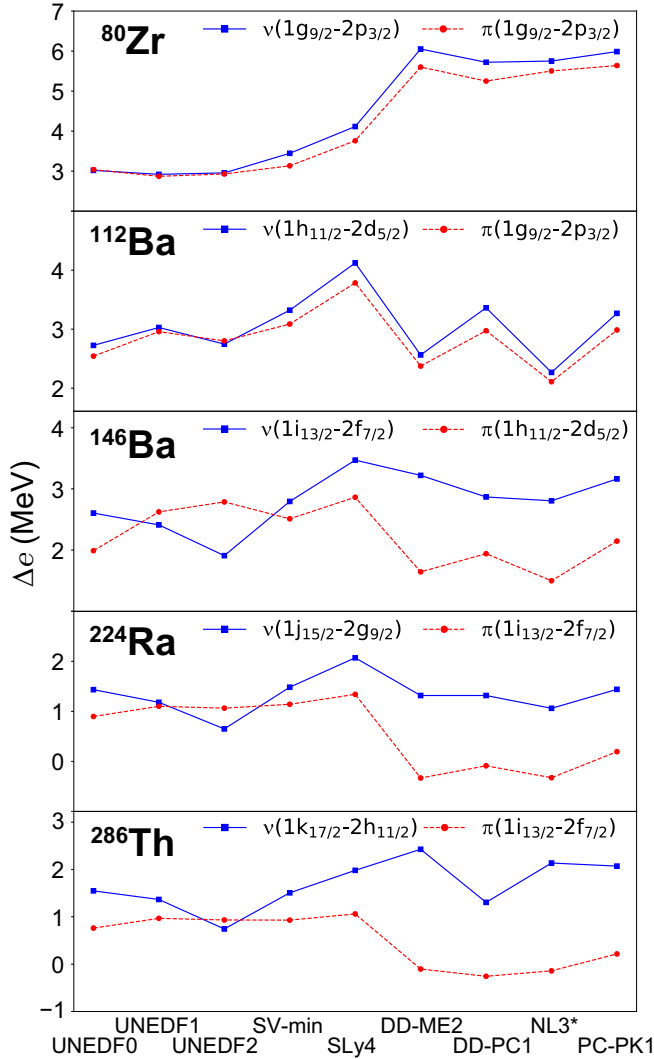


FIG. 3. Single-particle energy splitting Δe between the unusual-parity intruder shell (ℓ, j) and the normal-parity shell ($\ell - 3, j - 3$) for five nuclei representing different regions of octupole instability. The s.p. canonical states were obtained from spherical HFB/RHB calculations. Neutron (proton) splittings are indicated by solid (dashed) lines.

between the regions of ΔE_{oct} and β_3 obtained by these two EDF families. This systematic effect is illustrated in Fig. 5, where dots represent the HFB predictions with $m \geq 3$, squares show the RHB predictions with $m \geq 2$, and diamonds show the overlap of the two. This shift has been noted in Ref. [24] pertaining to superheavy nuclei.

IV. LOCAL TRENDS

The majority of octupole-deformed nuclei are found near the intersection between neutron numbers 88, 134, and 194 and proton numbers 56 and 88. This pattern is more pronounced in heavy nuclei, due to their lower values of Δe (see Fig. 3).

We note that all of the EDFs used in this study provide robust and consistent predictions for quadrupole moments,

which generally agree well with available experimental data ([68–70]; also see [67]). This suggests that the quadrupole collectivity is well developed. On the other hand, in many nuclei, the octupole deformation energy has a modest value of less than 500 keV. Such small values of ΔE_{oct} indicate soft PESs resulting in an octupole collectivity of transitional character, i.e., between octupole rotational and vibrational motions [8]. While in this work we refer to a nucleus as octupole deformed when its g.s. has $\beta_3 \neq 0$, this does not mean that this octupole deformation is static. For octupole-soft, transitional nuclei, beyond-mean-field methods are needed to describe the system [15,17,18,25,44–47].

In the following, we discuss the local regions of octupole collectivity with a focus on the cases robustly predicted to be octupole deformed in Skyrme EDF calculations. A detailed discussion of CEDF results can be found in Refs. [23,24]. Note that this discussion is not intended to provide a comprehensive review. For a detailed experimental discussion and other recent calculations we refer the reader to Refs. [9] and Refs. [13], [14], [20], and [25], respectively.

A. Neutron-deficient actinides

Because of their large octupole correlation effects and experimental accessibility, neutron-deficient actinides have traditionally been in the spotlight of octupole deformation studies. As shown in Fig. 4, this region is abundant in octupole-deformed nuclei, with many systems predicted robustly by several models, i.e., having a high octupole multiplicity. Figure 6 summarizes our SEDF results for the isotopic chains of Rn, Ra, Th, and U.

The isotopes $^{218,220}\text{Rn}$ and $^{224,226}\text{Rn}$ have been found experimentally to be close to the octupole vibrational limit [68,71–73]. As shown in Fig. 6(a), $|\Delta E_{\text{oct}}|$ reaches its maximum for ^{220}Rn , with an average value around -0.5 MeV. These shallow octupole minima suggest that neutron-deficient Rn isotopes are transitional systems, consistent with experiment.

The search for octupole instability in neutron-deficient Ra isotopes has been of great interest [9,68,74] also because of atomic EDM studies. According to numerous theoretical calculations, ^{224}Ra has the largest octupole deformation [9,74] and is often predicted to have the largest ΔE_{oct} among the Ra isotopes. It is therefore hardly surprising that ^{224}Ra , along with ^{226}Ra , is predicted to be octupole deformed by all nine energy density functionals studied.

Within the SEDFs, the values of β_2 , β_3 , and ΔE_{oct} appear to be very consistent for $^{220,222,224}\text{Ra}$ [cf. Fig. 6(b)]. The largest $|\Delta E_{\text{oct}}|$ is predicted for ^{222}Ra , followed by ^{220}Ra and ^{224}Ra . Recent experiments suggest that ^{222}Ra has the largest octupole deformation among the Ra isotopes, followed by ^{226}Ra , ^{228}Ra , and ^{224}Ra [74].

Experimentally, even-even $^{222-226}\text{Th}$ exhibit many signatures of stable octupole deformation [71,75,76], in agreement with the SEDFs' predictions shown in Fig. 6(c). All SEDFs predict octupole deformations in $^{220,222,224,226,228}\text{Th}$.

The majority of SEDFs predict even-even $^{222-228}\text{U}$ to be octupole deformed. As shown in Fig. 6(d), the highest octupole deformation energy, exceeding 2 MeV, is calculated

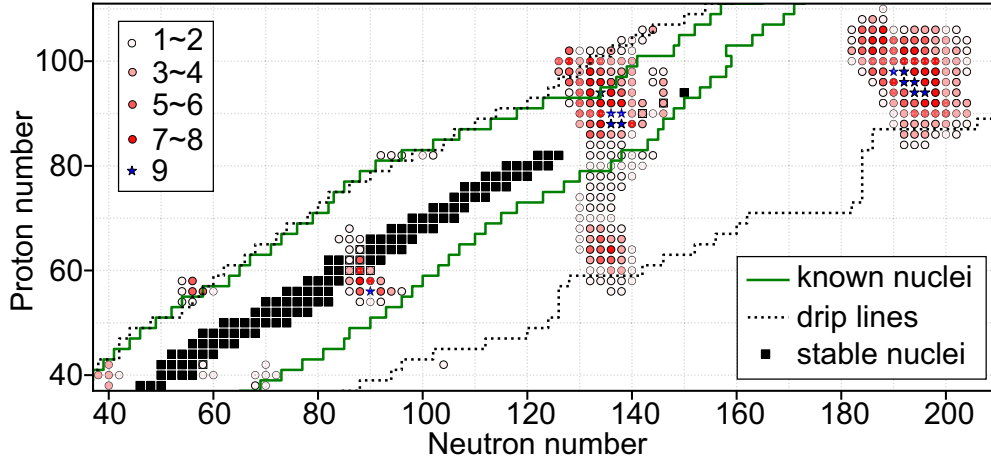


FIG. 4. The landscape of g.s. octupole deformations in even-even nuclei. Circles and stars represent nuclei predicted to have nonzero octupole deformations. The model multiplicity $m(Z, N)$ is indicated in the legend. The boundary of known (i.e., experimentally discovered) nuclei is shown by the solid line. For simplicity, this boundary is defined by the lightest and heaviest isotopes discovered for a given element. The average two-nucleon drip lines from Bayesian machine learning studies [64,65] are shown by dotted lines. Primordial nuclides [66] are indicated by squares.

for ^{224}U , followed by $^{222,226}\text{U}$. Experimentally, the nucleus ^{226}U has octupole characteristics similar to those of ^{222}Ra and ^{224}Th [77]. According to our study, the nucleus ^{224}U is a superb candidate for a pear-shaped system.

Neutron-deficient Pu isotopes have received little attention in octupole-instability studies, as they are extremely difficult to access. The lightest known Pu isotope, ^{228}Pu , has a half-life of 1.1 s [78] but spectroscopic information about this system is nonexistent. Likewise, virtually nothing is known about $^{230,232,234}\text{Pu}$, except for their g.s. properties [66]. Interestingly the isotope ^{228}Pu is predicted by all our models to be octupole deformed, followed by ^{226}Pu ($m = 7$) and ^{230}Pu ($m = 8$). The large values of $|\Delta E_{\text{oct}}|$ in $^{224,226,228}\text{Pu}$ (1.5–2 MeV) calculated by SEDFs are similar to those for Ra, Th, and U isotopes that show evidence of stable octupole deformations.

The lightest Cm isotope known experimentally is ^{233}Cm , which is significantly heavier than our best Cm candidates for pearlike shapes: $^{228,230}\text{Cm}$. As shown in Fig. 4, in neutron-deficient actinides with $Z \geq 98$, most of the best candidates for octupole deformation lie well beyond the current discovery range, and some appear to be close to, or outside, the predicted two-proton drip line [64].

B. Neutron-rich lanthanides

The region of Ba, Ce, Nd, and Sm isotopes around ^{146}Ba constitutes the second largest concentration of octupole-unstable nuclei predicted theoretically that are within experimental range. Figure 7 summarizes our SEDF results for the isotopic chains of Ba, Ce, and Nd.

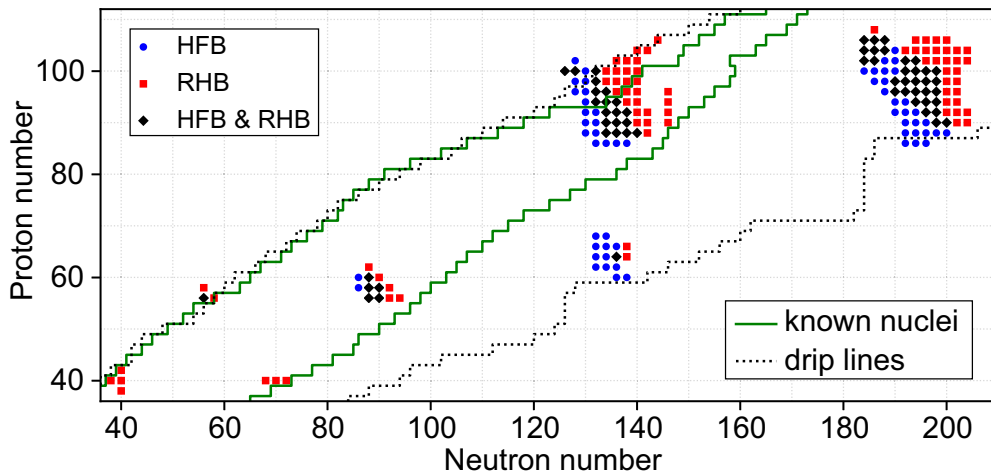


FIG. 5. Comparison between HFB and RHB predictions. Dots represent the HFB predictions with $m \geq 3$, squares show the RHB predictions with $m \geq 2$, and diamonds show the overlap region between HFB and RHB results. The borders of known nuclei and two-particle drip lines are as in Fig. 4.

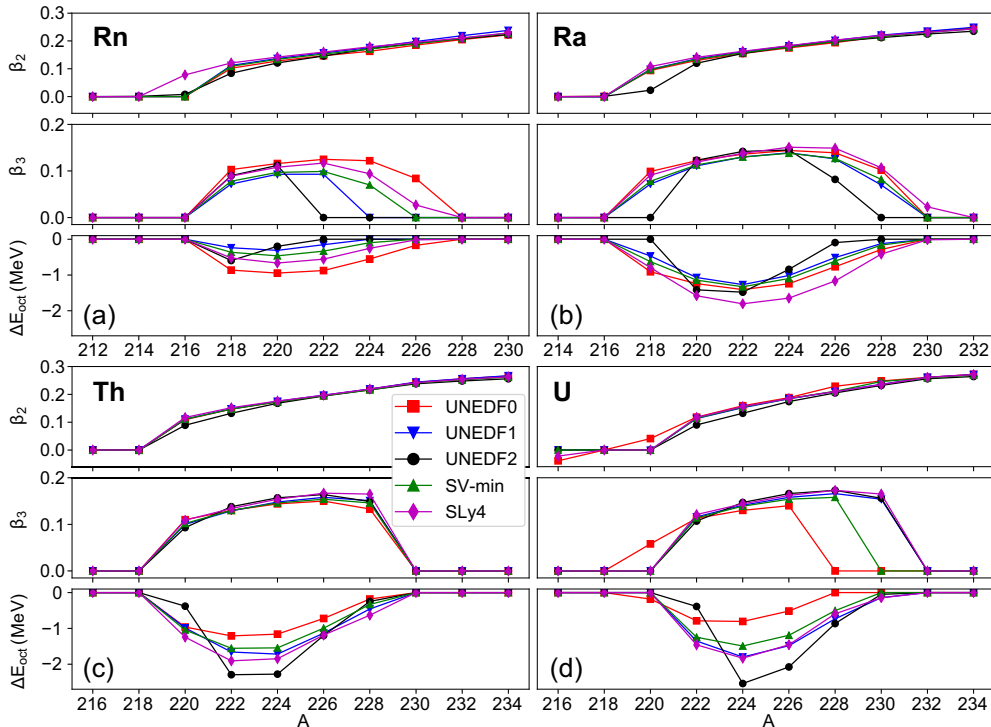


FIG. 6. Values of β_2 , β_3 , and ΔE_{oct} predicted by the SEDF models for the isotopic chains of (a) Rn, (b) Ra, (c) Th, and (d) U.

Intrinsic dipole moment measurements indicate appreciable octupole correlations in even-even $^{140-148}\text{Ba}$ [79–82]. In particular, direct measurements of E3 transition strength made recently in $^{144,146}\text{Ba}$ [83,84] suggest similar octupole correlations in these nuclei (within large experimental uncertainties). As shown in Fig. 7(a), except for UNEDF1, the SEDF results are consistent with this discovery in predicting similar β_3 and ΔE_{oct} for these isotopes.

For the Ce isotopes, all SEDFs except UNEDF0 predict octupole deformations in $^{146,148}\text{Ce}$, with the largest $|\Delta E_{\text{oct}}|$ in ^{146}Ce [see Fig. 7(b)]. Experiment suggests enhanced octupole correlations in ^{146}Ce [85], ^{144}Ce [81,85], and ^{148}Ce [86] and a weakened octupole collectivity in ^{150}Ce [87].

The stable isotopes $^{146,148}\text{Nd}$ are predicted to be octupole deformed. Experimental data suggest enhanced octupole collectivity in $^{146,148,150}\text{Nd}$ [88–92]. Another stable isotope with a high octupole multiplicity is ^{150}Sm . Experimentally, there is some evidence of octupole collectivity in an excited band of ^{150}Sm [93]. As shown in Fig. 4, the isotopes $^{146,148,150}\text{Nd}$ and ^{150}Sm are the only stable even-even candidates for octupole instability. The parity doublets in odd-mass nuclei from this region, such as ^{153}Eu , could be excellent candidates for searches of T,P -violating effects with atoms, ions, and molecules [94].

C. Proton-rich nuclei around ^{112}Ba

Strong octupole correlations, including octupole instability, were predicted theoretically in nuclei around ^{112}Ba in the early 1990s [95,96]. As shown in Fig. 4, some of our models yield reflection-asymmetric shapes in a handful of nuclei from this region that lie close to, or beyond, the proton drip line,

with ^{112}Ba being the best candidate. The experimental data in this region are scarce, with enhanced octupole correlations being suggested for ^{112}Xe [97] and ^{114}Xe [98]. The lightest observed Ba isotope is ^{114}Ba [99], for which no spectroscopic information exists.

D. Proton-rich and neutron-rich zirconium regions

Shallow octupole minima are calculated in the Zr region around $N = 40$ and $N = 70$ by some CEDFs (see Fig. 5) and also by Gogny calculations in Ref. [14]. On the other hand, our SEDF models predict no octupole instability in this region.

E. Very neutron-rich nuclei around ^{200}Gd

Many extremely neutron-rich nuclei around ^{200}Gd are predicted to be octupole deformed (see Fig. 4 and Supplemental Material [67]). While this region lies well outside experimental reach, nucleosynthesis calculations suggest that it can be accessed in a very neutron-rich r process [100]. The best candidates for octupole instability in this region are $^{196,198,200}\text{Sm}$, $^{196,198,200}\text{Gd}$, and ^{200}Dy .

F. Very neutron-rich nuclei around ^{288}Pu

Many extremely neutron-rich actinide and transactinide nuclei with $184 < N < 206$ are predicted to be pear shaped (see Fig. 4 and Refs. [16,19,22,24]). From a purely nuclear structure perspective, this broad region of octupole instability is of solely theoretical interest as it lies well outside experimental reach. While the production of nuclei heavier than $N = 184$ in the astrophysical r process is expected to be strongly hindered by neutron-induced fission [42,101], the magnitude

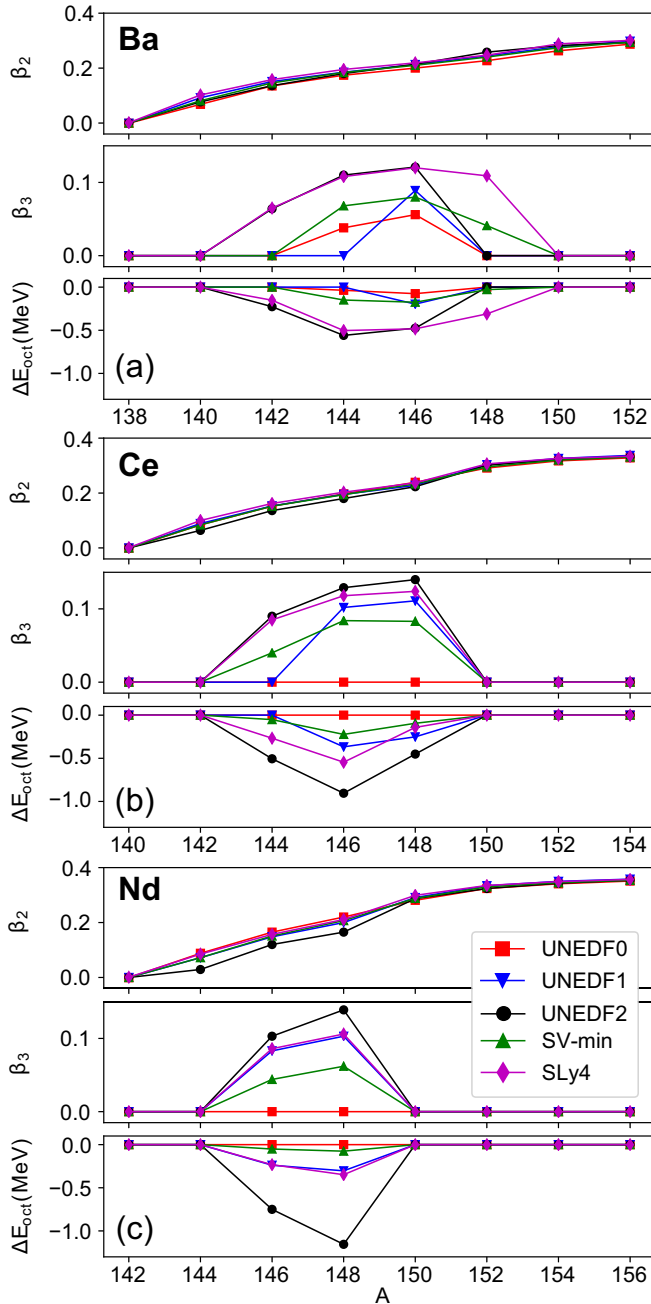


FIG. 7. Similar to Fig. 6, but for (a) Ba, (b) Ce, and (c) Nd.

of this suppression strongly depends on the predicted fission barriers [102] and hence the question of their astrophysical relevance is still open.

V. SUMMARY

A systematic survey of reflection-asymmetric, axially symmetric even-even nuclei has been carried out within the Skyrme-HFB approach. Among the five SEDFs employed, UNEDF2 and SLy4 predict the largest number of octupole-deformed nuclei and, also, the highest octupole deformation energies ΔE_{oct} . The functional UNEDF0, which was not optimized to experimental shell gaps, predicts the lowest

number of octupole minima. This can be attributed to the larger energy splitting $\Delta\epsilon$ between octupole-driving (ℓ, j) and $(\ell - 3, j - 3)$ shells in this model. The low values of $\Delta\epsilon$ are indicative of enhanced octupole correlations. However, these quantities are not instrumental in the predictions of their magnitude.

These results are combined with those obtained with four CEDFs in Refs. [23,24] and additional RHB calculations performed for the present paper. This makes it possible to produce the landscape of octupole deformations shown in Fig. 4, which displays reflection-asymmetric nuclei for non-relativistic and relativistic EDFs, thus limiting systematic model uncertainties. There are 12 even-even nuclei predicted by all nine EDFs to be octupole deformed: ^{146}Ba , $^{224,226}\text{Ra}$, $^{226,228}\text{Th}$, ^{228}Pu , $^{288,290}\text{Pu}$, $^{288,290}\text{Cm}$, and $^{288,290}\text{Cf}$.

By analyzing the trend of β_2 , β_3 , and ΔE_{oct} along isotopic chains of actinides and lanthanides, we found that the SEDF results are fairly consistent with other studies [13–15]. The study in Ref. [20] predicted relatively few octupole-unstable nuclei, which was acknowledged by the authors as possibly being due to the strong pairing interaction. A shift in the position of octupole-unstable regions (by two to four neutron numbers) is seen when comparing the results of SEDF and CEDF models. This shift is shown in Fig. 5 and likely comes from the shell structure obtained with CEDF models, as the SEDF results agree well with the results of other global nonrelativistic surveys. Minor differences aside, the octupole landscape presented in Fig. 4 is consistent with current experimental data. Quadrupole deformations are highly consistent across all nine models used and agree well with experiment.

In the neutron-deficient actinide region, in addition to the “usual suspects,” our study suggests stable g.s. octupole deformations in $^{224,226,228}\text{U}$, $^{226,228,230}\text{Pu}$, and $^{228,230}\text{Cm}$. The only stable pear-shaped even-even nuclei expected theoretically are $^{146,148,150}\text{Nd}$ and ^{150}Sm .

Our global survey predicts two exotic regions of octupole instability in extremely neutron-rich nuclei that are inaccessible experimentally. The first region, of lanthanide nuclei around ^{200}Gd , is possibly populated in a very neutron-rich r process. In the second region, of actinide and transactinide nuclei with $184 < N < 206$, neutron-induced fission is likely to suppress the r -process production of nuclei with $N > 184$, but the magnitude of this hindrance strongly depends on the predicted fission barriers.

It will be of great interest to expand this work with systematic DFT studies of octupole deformation and an underlying single-particle structure in odd-mass and odd-odd nuclei. Progress has been made in exploring particle-odd systems by using projection techniques, primarily in the systematic computation of Schiff moments [35], but much work still remains to be done.

ACKNOWLEDGMENTS

Discussions with Jacek Dobaczewski and Samuel Giuliani are greatly appreciated. Computational resources were provided by the Institute for Cyber-Enabled Research at Michigan State University. This material is based upon work supported by the U.S. Department of Energy, Office of Science,

Office of Nuclear Physics, under award nos. DE-SC0013365 (Michigan State University) and DE-SC0013037 (Mississippi State University), DE-SC0018083 (NUCLEI SciDAC-4 Collaboration), DOE-NA0003885 and DOE-NA0002925

(NNSA, the Stewardship Science Academic Alliances program), and DE-SC0015376 (DOE Topical Collaboration in Nuclear Theory for Double-Beta Decay and Fundamental Symmetries).

- [1] H. A. Jahn and E. Teller, Stability of polyatomic molecules in degenerate electronic states. I. Orbital degeneracy, *Proc. R. Soc. London A* **161**, 220 (1937).
- [2] P.-G. Reinhard and E. W. Otten, Transition to deformed shapes as a nuclear Jahn-Teller effect, *Nucl. Phys. A* **420**, 173 (1984).
- [3] W. Nazarewicz, Microscopic origin of nuclear deformations, *Nucl. Phys. A* **574**, 27 (1994).
- [4] S. Frauendorf, Spontaneous symmetry breaking in rotating nuclei, *Rev. Mod. Phys.* **73**, 463 (2001).
- [5] V. M. Strutinsky, Remarks about pear-shaped nuclei, *Physica* **22**, 1166 (1956).
- [6] K. Lee and D. R. Inglis, Stability of pear-shaped nuclear deformations, *Phys. Rev.* **108**, 774 (1957).
- [7] S. A. Johansson, Nuclear octupole deformation and the mechanism of fission, *Nucl. Phys.* **22**, 529 (1961).
- [8] P. A. Butler and W. Nazarewicz, Intrinsic reflection asymmetry in atomic nuclei, *Rev. Mod. Phys.* **68**, 349 (1996).
- [9] P. A. Butler, Octupole collectivity in nuclei, *J. Phys. G* **43**, 073002 (2016).
- [10] A. Gyurkovich, A. Sobczewski, B. Nerlo-Pomorska, and K. Pomorski, On the stable octupole deformation of nuclei, *Phys. Lett. B* **105**, 95 (1981).
- [11] W. Nazarewicz, P. Olanders, I. Ragnarsson, J. Dudek, G. Leander, P. Möller, and E. Ruchowska, Analysis of octupole instability in medium-mass and heavy nuclei, *Nucl. Phys. A* **429**, 269 (1984).
- [12] P. Möller, J. Nix, W. Myers, and W. Swiatecki, Nuclear ground-state masses and deformations, *At. Data Nucl. Data Tables* **59**, 185 (1995).
- [13] P. Möller, R. Bengtsson, B. G. Carlsson, P. Olivius, T. Ichikawa, H. Sagawa, and A. Iwamoto, Axial and reflection asymmetry of the nuclear ground state, *At. Data Nucl. Data Tables* **94**, 758 (2008).
- [14] L. M. Robledo and G. F. Bertsch, Global systematics of octupole excitations in even-even nuclei, *Phys. Rev. C* **84**, 054302 (2011).
- [15] L. M. Robledo and R. R. Rodríguez-Guzmán, Octupole deformation properties of actinide isotopes within a mean-field approach, *J. Phys. G* **39**, 105103 (2012).
- [16] M. Warda and J. L. Egido, Fission half-lives of superheavy nuclei in a microscopic approach, *Phys. Rev. C* **86**, 014322 (2012).
- [17] L. M. Robledo, Ground state octupole correlation energy with effective forces, *J. Phys. G* **42**, 055109 (2015).
- [18] L. M. Robledo, M. Baldo, P. Schuck, and X. Viñas, Octupole deformation properties of the Barcelona-Catania-Paris energy density functionals, *Phys. Rev. C* **81**, 034315 (2010).
- [19] J. Erler, K. Langanke, H. P. Loens, G. Martínez-Pinedo, and P.-G. Reinhard, Fission properties for r -process nuclei, *Phys. Rev. C* **85**, 025802 (2012).
- [20] S. Ebata and T. Nakatsukasa, Octupole deformation in the nuclear chart based on the 3D Skyrme Hartree-Fock plus BCS model, *Phys. Scripta* **92**, 064005 (2017).
- [21] K. Nomura, D. Vretenar, T. Nikšić, and B.-N. Lu, Microscopic description of octupole shape transitions in light actinide and rare-earth nuclei, *Phys. Rev. C* **89**, 024312 (2014).
- [22] Z. Xu and Z.-P. Li, Microscopic analysis of octupole shape transitions in neutron-rich actinides with relativistic energy density functional, *Chin. Phys. C* **41**, 124107 (2017).
- [23] S. E. Agbemava, A. V. Afanasjev, and P. Ring, Octupole deformation in the ground states of even-even nuclei: A global analysis within the covariant density functional theory, *Phys. Rev. C* **93**, 044304 (2016).
- [24] S. E. Agbemava and A. V. Afanasjev, Octupole deformation in the ground states of even-even $Z \sim 96$, $N \sim 196$ actinides and superheavy nuclei, *Phys. Rev. C* **96**, 024301 (2017).
- [25] S. Y. Xia, H. Tao, Y. Lu, Z. P. Li, T. Nikšić, and D. Vretenar, Spectroscopy of reflection-asymmetric nuclei with relativistic energy density functionals, *Phys. Rev. C* **96**, 054303 (2017).
- [26] W. C. Haxton and E. M. Henley, Enhanced T -Nonconserving Nuclear Moments, *Phys. Rev. Lett.* **51**, 1937 (1983).
- [27] W. C. Haxton, Atomic parity violation and the nuclear anapole moment, *Science* **275**, 1753 (1997).
- [28] T. E. Chupp, P. Fierlinger, M. J. Ramsey-Musolf, and J. T. Singh, Electric dipole moments of atoms, molecules, nuclei, and particles, *Rev. Mod. Phys.* **91**, 015001 (2019).
- [29] L. I. Schiff, Measurability of nuclear electric dipole moments, *Phys. Rev.* **132**, 2194 (1963).
- [30] N. Auerbach, V. V. Flambaum, and V. Spevak, Collective T - and P -Odd Electromagnetic Moments in Nuclei with Octupole Deformations, *Phys. Rev. Lett.* **76**, 4316 (1996).
- [31] V. Spevak, N. Auerbach, and V. V. Flambaum, Enhanced T -odd, P -odd electromagnetic moments in reflection asymmetric nuclei, *Phys. Rev. C* **56**, 1357 (1997).
- [32] J. Engel, J. L. Friar, and A. C. Hayes, Nuclear octupole correlations and the enhancement of atomic time-reversal violation, *Phys. Rev. C* **61**, 035502 (2000).
- [33] J. Engel, M. Bender, J. Dobaczewski, J. H. de Jesus, and P. Olbratowski, Time-reversal violating Schiff moment of ^{225}Ra , *Phys. Rev. C* **68**, 025501 (2003).
- [34] V. V. Flambaum, Enhanced nuclear Schiff moment and time-reversal violation in ^{229}Th -containing molecules, *Phys. Rev. C* **99**, 035501 (2019).
- [35] J. Dobaczewski, J. Engel, M. Kortelainen, and P. Becker, Correlating Schiff Moments in the Light Actinides with Octupole Moments, *Phys. Rev. Lett.* **121**, 232501 (2018).
- [36] M. Bender, P.-H. Heenen, and P.-G. Reinhard, Self-consistent mean-field models for nuclear structure, *Rev. Mod. Phys.* **75**, 121 (2003).
- [37] J. Erler, N. Birge, M. Kortelainen, W. Nazarewicz, E. Olsen, A. M. Perhac, and M. Stoitsov, The limits of the nuclear landscape, *Nature* **486**, 509 (2012).
- [38] A. V. Afanasjev and S. Frauendorf, Central depression in nuclear density and its consequences for the shell structure of superheavy nuclei, *Phys. Rev. C* **71**, 024308 (2005).

- [39] B. Schuetrumpf, W. Nazarewicz, and P.-G. Reinhard, Central depression in nucleonic densities: Trend analysis in the nuclear density functional theory approach, *Phys. Rev. C* **96**, 024306 (2017).
- [40] W. Nazarewicz, The limits of nuclear mass and charge, *Nat. Phys.* **14**, 537 (2018).
- [41] A. V. Afanasjev, S. E. Agbemava, and A. Gyawali, Hyperheavy nuclei: Existence and stability, *Phys. Lett. B* **782**, 533 (2018).
- [42] S. A. Giuliani, Z. Matheson, W. Nazarewicz, E. Olsen, P.-G. Reinhard, J. Sadhukhan, B. Schuetrumpf, N. Schunck, and P. Schwerdtfeger, Colloquium: Superheavy elements: Oganesson and beyond, *Rev. Mod. Phys.* **91**, 011001 (2019).
- [43] S. E. Agbemava, A. V. Afanasjev, A. Taninah, and A. Gyawali, Extension of the nuclear landscape to hyperheavy nuclei, *Phys. Rev. C* **99**, 034316 (2019).
- [44] J. Egido and L. Robledo, Parity-projected calculations on octupole deformed nuclei, *Nucl. Phys. A* **524**, 65 (1991).
- [45] L. M. Robledo, Enhancement of octupole strength in near spherical nuclei, *Eur. Phys. J. A* **52**, 300 (2016).
- [46] J. M. Yao, E. F. Zhou, and Z. P. Li, Beyond relativistic mean-field approach for nuclear octupole excitations, *Phys. Rev. C* **92**, 041304 (2015).
- [47] J. M. Yao and J. Engel, Octupole correlations in low-lying states of ^{150}Nd and ^{150}Sm and their impact on neutrinoless double- β decay, *Phys. Rev. C* **94**, 014306 (2016).
- [48] M. Kortelainen, T. Lesinski, J. Moré, W. Nazarewicz, J. Sarich, N. Schunck, M. V. Stoitsov, and S. Wild, Nuclear energy density optimization, *Phys. Rev. C* **82**, 024313 (2010).
- [49] M. Kortelainen, J. McDonnell, W. Nazarewicz, P.-G. Reinhard, J. Sarich, N. Schunck, M. V. Stoitsov, and S. M. Wild, Nuclear energy density optimization: Large deformations, *Phys. Rev. C* **85**, 024304 (2012).
- [50] M. Kortelainen, J. McDonnell, W. Nazarewicz, E. Olsen, P.-G. Reinhard, J. Sarich, N. Schunck, S. M. Wild, D. Davesne, J. Erler, and A. Pastore, Nuclear energy density optimization: Shell structure, *Phys. Rev. C* **89**, 054314 (2014).
- [51] E. Chabanat, P. Bonche, P. Haensel, J. Meyer, and R. Schaeffer, New Skyrme effective forces for supernovae and neutron rich nuclei, *Phys. Scr.* **1995**, 231 (1995).
- [52] P. Klüpfel, P.-G. Reinhard, T. J. Bürvenich, and J. A. Maruhn, Variations on a theme by Skyrme: A systematic study of adjustments of model parameters, *Phys. Rev. C* **79**, 034310 (2009).
- [53] M. Wang, G. Audi, F. G. Kondev, W. Huang, S. Naimi, and X. Xu, The AME2016 atomic mass evaluation. II. Tables, graphs and references, *Chin. Phys. C* **41**, 030003 (2017).
- [54] J. Dobaczewski, W. Nazarewicz, and M. Stoitsov, Nuclear ground-state properties from mean-field calculations, *Eur. Phys. J. A* **15**, 21 (2002).
- [55] M. V. Stoitsov, J. Dobaczewski, W. Nazarewicz, S. Pittel, and D. J. Dean, Systematic study of deformed nuclei at the drip lines and beyond, *Phys. Rev. C* **68**, 054312 (2003).
- [56] R. N. Perez, N. Schunck, R.-D. Lasserri, C. Zhang, and J. Sarich, Axially deformed solution of the Skyrme-Hartree-Fock-Bogolyubov equations using the transformed harmonic oscillator basis (iii) HFBTHO (v3.00): A new version of the program, *Comput. Phys. Commun.* **220**, 363 (2017).
- [57] D. Vretenar, A. V. Afanasjev, G. A. Lalazissis, and P. Ring, Relativistic Hartree-Bogoliubov theory: Static and dynamic aspects of exotic nuclear structure, *Phys. Rep.* **409**, 101 (2005).
- [58] G. A. Lalazissis, T. Nikšić, D. Vretenar, and P. Ring, New relativistic mean-field interaction with density-dependent meson-nucleon couplings, *Phys. Rev. C* **71**, 024312 (2005).
- [59] G. A. Lalazissis, S. Karatzikos, R. Fossion, D. P. Arteaga, A. V. Afanasjev, and P. Ring, The effective force NL3 revisited, *Phys. Lett. B* **671**, 36 (2009).
- [60] P. W. Zhao, Z. P. Li, J. M. Yao, and J. Meng, New parametrization for the nuclear covariant energy density functional with a point-coupling interaction, *Phys. Rev. C* **82**, 054319 (2010).
- [61] T. Nikšić, D. Vretenar, and P. Ring, Relativistic nuclear energy density functionals: Adjusting parameters to binding energies, *Phys. Rev. C* **78**, 034318 (2008).
- [62] S. E. Agbemava, A. V. Afanasjev, D. Ray, and P. Ring, Global performance of covariant energy density functionals: Ground state observables of even-even nuclei and the estimate of theoretical uncertainties, *Phys. Rev. C* **89**, 054320 (2014).
- [63] Y. Tian, Z. Ma, and P. Ring, A finite range pairing force for density functional theory in superfluid nuclei, *Phys. Lett. B* **676**, 44 (2009).
- [64] L. Neufcourt, Y. Cao, S. A. Giuliani, W. Nazarewicz, E. Olsen, and O. B. Tarasov, Quantified limits of the nuclear landscape, *Phys. Rev. C* **101**, 044307 (2020).
- [65] L. Neufcourt, Y. Cao, S. A. Giuliani, W. Nazarewicz, E. Olsen, and O. B. Tarasov, Beyond the proton drip line: Bayesian analysis of proton-emitting nuclei, *Phys. Rev. C* **101**, 014319 (2020).
- [66] National Nuclear Data Center, <http://www.nndc.bnl.gov>.
- [67] See Supplemental Material at <http://link.aps.org/supplemental/10.1103/PhysRevC.102.024311> for the predicted values of ΔE_{oct} and β_3 for nuclei with octupole multiplicity $m \geq 6$ and the proton quadrupole and octupole moments.
- [68] L. P. Gaffney, P. A. Butler, M. Scheck, A. B. Hayes, F. Wenander, M. Albers, B. Bastin, C. Bauer, A. Blazhev, S. Bönig, N. Bree, J. Cederkäll, T. Chupp, D. Cline, T. E. Cocolios, T. Davinson, H. de Witte, J. Diriken, T. Grahn, A. Herzan, M. Huysse, D. G. Jenkins, D. T. Joss, N. Kesteloot, J. Konki, M. Kowalczyk, T. Kröll, E. Kwan, R. Lutter, K. Moschner, P. Napiorkowski, J. Pakarinen, M. Pfeiffer, D. Radeck, P. Reiter, K. Reynders, S. V. Rigby, L. M. Robledo, M. Rudigier, S. Sambri, M. Seidlitz, B. Siebeck, T. Stora, P. Thoele, P. van Duppen, M. J. Vermeulen, M. von Schmid, D. Voulot, N. Warr, K. Wimmer, K. Wrzosek-Lipska, C. Y. Wu, and M. Zielinska, Studies of pear-shaped nuclei using accelerated radioactive beams, *Nature (London)* **497**, 199 (2013).
- [69] K. Gulda, H. Mach, A. Aas, M. Borge, D. Burke, B. Fogelberg, H. Gietz, I. Grant, E. Hagebo, P. Hill, P. Hoff, N. Kaffrell, W. Kurciewicz, A. Lindroth, G. Løvholm, T. Martinez, S. Mattsson, R. Naumann, K. Nybø, G. Nyman, B. Rubio, M. Sanchez-Vega, J. Tain, R. Taylor, O. Tengblad, and T. Thorsteinsen, Quadrupole deformed and octupole collective bands in ^{228}Ra , *Nucl. Phys. A* **636**, 28 (1998).
- [70] S. Singh, A. Jain, and J. K. Tuli, Nuclear data sheets for $A = 222$, *Nucl. Data Sheets* **112**, 2851 (2011).
- [71] J. F. C. Cocks, P. A. Butler, K. J. Cann, P. T. Greenlees, G. D. Jones, S. Asztalos, P. Bhattacharyya, R. Broda, R. M. Clark, M. A. Deleplanque, R. M. Diamond, P. Fallon, B. Fornal, P. M. Jones, R. Julin, T. Lauritsen, I. Y. Lee, A. O. Macchiavelli, R. W. MacLeod, J. F. Smith, F. S. Stephens, and C. T. Zhang, Observation of Octupole Structures in Radon and Radium

- Isotopes and Their Contrasting Behavior at High Spin, *Phys. Rev. Lett.* **78**, 2920 (1997).
- [72] J. Cocks, D. Hawcroft, N. Amzal, P. Butler, K. Cann, P. Greenlees, G. Jones, S. Asztalos, R. Clark, M. Deleplanque, R. Diamond, P. Fallon, I. Lee, A. Macchiavelli, R. MacLeod, F. Stephens, P. Jones, R. Julin, R. Broda, B. Fornal, J. Smith, T. Lauritsen, P. Bhattacharyya, and C. Zhang, Spectroscopy of Rn, Ra and Th isotopes using multi-nucleon transfer reactions, *Nucl. Phys. A* **645**, 61 (1999).
- [73] P. A. Butler, L. P. Gaffney, P. Spagnoletti, J. Konki, M. Scheck, J. F. Smith, K. Abrahams, M. Bowry, J. Cederkäll, T. Chupp, G. de Angelis, H. De Witte, P. E. Garrett, A. Goldkuhle, C. Henrich, A. Illana, K. Johnston, D. T. Joss, J. M. Keatings, N. A. Kelly, M. Komorowska, T. Kröll, M. Lozano, B. S. Nara Singh, D. O'Donnell, J. Ojala, R. D. Page, L. G. Pedersen, C. Raison, P. Reiter, J. A. Rodriguez, D. Rosiak, S. Rothe, T. M. Shneidman, B. Siebeck, M. Seidlitz, J. Sinclair, M. Stryjczyk, P. Van Duppen, S. Vinals, V. Virtanen, N. Warr, K. Wrzosek-Lipska, and M. Zielinska, The observation of vibrating pear-shapes in radon nuclei, *Nat. Commun.* **10**, 2473 (2019).
- [74] P. A. Butler, L. P. Gaffney, P. Spagnoletti, K. Abrahams, M. Bowry, J. Cederkäll, G. de Angelis, H. De Witte, P. E. Garrett, A. Goldkuhle, C. Henrich, A. Illana, K. Johnston, D. T. Joss, J. M. Keatings, N. A. Kelly, M. Komorowska, J. Konki, T. Kröll, M. Lozano, B. S. Nara Singh, D. O'Donnell, J. Ojala, R. D. Page, L. G. Pedersen, C. Raison, P. Reiter, J. A. Rodriguez, D. Rosiak, S. Rothe, M. Scheck, M. Seidlitz, T. M. Shneidman, B. Siebeck, J. Sinclair, J. F. Smith, M. Stryjczyk, P. Van Duppen, S. Vinals, V. Virtanen, N. Warr, K. Wrzosek-Lipska, and M. Zielińska, Evolution of Octupole Deformation in Radium Nuclei from Coulomb Excitation of Radioactive ^{222}Ra and ^{228}Ra Beams, *Phys. Rev. Lett.* **124**, 042503 (2020).
- [75] B. Ackermann, H. Baltzer, C. Ensel, K. Freitag, V. Grafen, C. Günther, P. Herzog, J. Manns, M. Marten-Tölle, U. Müller, J. Prinz, I. Romanski, R. Tölle, J. deBoer, N. Gollwitzer, and H. Maier, Collective E1 transitions in even-A Ra, Th, and U nuclei, *Nucl. Phys. A* **559**, 61 (1993).
- [76] J. F. Smith, J. F. C. Cocks, N. Schulz, M. Aïche, M. Bentaleb, P. A. Butler, F. Hannachi, G. D. Jones, P. M. Jones, R. Julin, S. Juutinen, R. Kulesa, E. Lubkiewicz, A. Płochocki, F. Riess, E. Ruchowska, A. Savelius, J. C. Sens, J. Simpson, and E. Wolf, Contrasting Behavior in Octupole Structures Observed at High Spin in ^{220}Ra and ^{222}Th , *Phys. Rev. Lett.* **75**, 1050 (1995).
- [77] P. T. Greenlees, N. Amzal, P. A. Butler, K. J. Cann, D. Hawcroft, G. D. Jones, R. D. Page, J. F. C. Cocks, A. Andreev, T. Enqvist, K. Helariutta, P. M. Jones, R. Julin, S. Juutinen, H. Kankaanpää, H. Kettunen, P. Kuusiniemi, M. Leino, M. Muikku, A. Savelius, W. H. Trzaska, J. Uusitalo, P. Fallon, B. Gall, F. Hoellinger, M. Guttormsen, S. Messelt, A. Schiller, S. Siem, and T. Tveter, First observation of excited states in ^{226}U , *J. Phys. G* **24**, L63 (1998).
- [78] K. Nishio, H. Ikezoe, S. Mitsuoka, K. Satou, and C. J. Lin, Half-life of ^{228}Pu and α decay of ^{228}Np , *Phys. Rev. C* **68**, 064305 (2003).
- [79] W. R. Phillips, I. Ahmad, H. Emling, R. Holzmann, R. V. F. Janssens, T. L. Khoo, and M. W. Drigert, Octupole Deformation in Neutron-Rich Barium Isotopes, *Phys. Rev. Lett.* **57**, 3257 (1986).
- [80] H. Mach, W. Nazarewicz, D. Kusnezov, M. Moszyński, B. Fogelberg, M. Hellström, L. Spanier, R. L. Gill, R. F. Casten, and A. Wolf, Influence of shell effects and stable octupole deformation on the E1 and E2 transition rates in the heavy-Ba region, *Phys. Rev. C* **41**, 2469(R) (1990).
- [81] S. Zhu, Q. Lu, J. Hamilton, A. Ramayya, L. Peker, M. Wang, W. Ma, B. Babu, T. Ginter, J. Kormicki, D. Shi, J. Deng, W. Nazarewicz, J. Rasmussen, M. Stoyer, S. Chu, K. Gregorich, M. Mohar, S. Asztalos, S. Prussin, J. Cole, R. Aryaeinejad, Y. Dardenne, M. Drigert, K. Moody, R. Loughed, J. Wild, N. Johnson, I. Lee, F. McGowan, G. Ter-Akopian, and Y. Oganessian, Octupole deformation in $^{142,143}\text{Ba}$ and ^{144}Ce : New band structures in neutron-rich Ba-isotopes, *Phys. Lett. B* **357**, 273 (1995).
- [82] W. Urban, M. Jones, J. Durell, M. Leddy, W. Phillips, A. Smith, B. Varley, I. Ahmad, L. Morss, M. Bentaleb, E. Lubkiewicz, and N. Schulz, Octupole correlations in neutron-rich, even-even barium isotopes, *Nucl. Phys. A* **613**, 107 (1997).
- [83] B. Bucher, S. Zhu, C. Y. Wu, R. V. F. Janssens, D. Cline, A. B. Hayes, M. Albers, A. D. Ayangeakaa, P. A. Butler, C. M. Campbell, M. P. Carpenter, C. J. Chiara, J. A. Clark, H. L. Crawford, M. Cromaz, H. M. David, C. Dickerson, E. T. Gregor, J. Harker, C. R. Hoffman, B. P. Kay, F. G. Kondev, A. Korichi, T. Lauritsen, A. O. Macchiavelli, R. C. Pardo, A. Richard, M. A. Riley, G. Savard, M. Scheck, D. Seweryniak, M. K. Smith, R. Vondrasek, and A. Wiens, Direct Evidence of Octupole Deformation in Neutron-Rich ^{144}Ba , *Phys. Rev. Lett.* **116**, 112503 (2016).
- [84] B. Bucher, S. Zhu, C. Y. Wu, R. V. F. Janssens, R. N. Bernard, L. M. Robledo, T. R. Rodríguez, D. Cline, A. B. Hayes, A. D. Ayangeakaa, M. Q. Buckner, C. M. Campbell, M. P. Carpenter, J. A. Clark, H. L. Crawford, H. M. David, C. Dickerson, J. Harker, C. R. Hoffman, B. P. Kay, F. G. Kondev, T. Lauritsen, A. O. Macchiavelli, R. C. Pardo, G. Savard, D. Seweryniak, and R. Vondrasek, Direct Evidence for Octupole Deformation in ^{146}Ba and the Origin of Large E1 Moment Variations in Reflection-Asymmetric Nuclei, *Phys. Rev. Lett.* **118**, 152504 (2017).
- [85] W. Phillips, R. Janssens, I. Ahmad, H. Emling, R. Holzmann, T. Khoo, and M. Drigert, Octupole correlation effects near $Z = 56$, $N = 88$, *Phys. Lett. B* **212**, 402 (1988).
- [86] Y. J. Chen, S. J. Zhu, J. H. Hamilton, A. V. Ramayya, J. K. Hwang, M. Sakhæe, Y. X. Luo, J. O. Rasmussen, K. Li, I. Y. Lee, X. L. Che, H. B. Ding, and M. L. Li, Search for octupole correlations in neutron-rich ^{148}Ce nucleus, *Phys. Rev. C* **73**, 054316 (2006).
- [87] S. J. Zhu, M. Sakhæe, J. H. Hamilton, A. V. Ramayya, N. T. Brewer, J. K. Hwang, S. H. Liu, E. Y. Yeoh, Z. G. Xiao, Q. Xu, Z. Zhang, Y. X. Luo, J. O. Rasmussen, I. Y. Lee, K. Li, and W. C. Ma, Observation of new levels and proposed octupole correlations in neutron-rich ^{150}Ce , *Phys. Rev. C* **85**, 014330 (2012).
- [88] W. Urban, R. Lieder, J. Bacelar, P. Singh, D. Alber, D. Balabanski, W. Gast, H. Grawe, G. Hebbinghaus, J. Jongman, T. Morek, R. Noorman, T. Rzaca-Urban, H. Schnare, M. Thoms, O. Zell, and W. Nazarewicz, High-spin octupole correlations in the $N = 86$, ^{146}Nd and ^{148}Sm nuclei, *Phys. Lett. B* **258**, 293 (1991).
- [89] V. Jacob, W. Urban, J. Bacelar, J. Jongman, J. Nyberg, G. Sletten, and L. Trache, Reflection asymmetric states in ^{146}Nd , *Nucl. Phys. A* **596**, 155 (1996).

- [90] R. Ibbotson, C. A. White, T. Czosnyka, P. A. Butler, N. Clarkson, D. Cline, R. A. Cunningham, M. Devlin, K. G. Helmer, T. H. Hoare, J. R. Hughes, G. D. Jones, A. E. Kavka, B. Kotlinski, R. J. Poynter, P. Regan, E. G. Vogt, R. Wadsworth, D. L. Watson, and C. Y. Wu, Octupole Collectivity in the Ground Band of ^{148}Nd , *Phys. Rev. Lett.* **71**, 1990 (1993).
- [91] R. Ibbotson, C. White, T. Czosnyka, P. Butler, N. Clarkson, D. Cline, R. Cunningham, M. Devlin, K. Helmer, T. Hoare, J. Hughes, G. Jones, A. Kavka, B. Kotlinski, R. Poynter, P. Regan, E. Vogt, R. Wadsworth, D. Watson, and C. Wu, Quadrupole and octupole collectivity in ^{148}Nd , *Nucl. Phys. A* **619**, 213 (1997).
- [92] H. Friedrichs, B. Schlitt, J. Margraf, S. Lindenstruth, C. Wesselborg, R. D. Heil, H. H. Pitz, U. Kneissl, P. von Brentano, R. D. Herzberg, A. Zilges, D. Hager, G. Muller, and M. Schumacher, Evidence for enhanced electric dipole excitations in deformed rare earth nuclei near 2.5 MeV, *Phys. Rev. C* **45**, 892(R) (1992).
- [93] S. P. Bvumbi, J. F. Sharpey-Schafer, P. M. Jones, S. M. Mullins, B. M. Nyako, K. Juhasz, R. A. Bark, L. Bianco, D. M. Cullen, D. Curien, P. E. Garrett, P. T. Greenlees, J. Hirvonen, U. Jakobsson, J. Kau, F. Komati, R. Julin, S. Juutinen, S. Ketelhut, A. Korichi, E. A. Lawrie, J. J. Lawrie, M. Leino, T. E. Madiba, S. N. T. Majola, P. Maine, A. Minkova, N. J. Ncapayi, P. Nieminen, P. Peura, P. Rahkila, L. L. Riedinger, P. Ruotsalainen, J. Saren, C. Scholey, J. Sorri, S. Stolze, J. Timar, J. Uusitalo, and P. A. Vymers, Octupole correlations in the structure of 0_2^+ bands in the $N = 88$ nuclei ^{150}Sm and ^{152}Gd , *Phys. Rev. C* **87**, 044333 (2013).
- [94] V. V. Flambaum and H. Feldmeier, Enhanced nuclear Schiff moment in stable and metastable nuclei, *Phys. Rev. C* **101**, 015502 (2020).
- [95] J. Skalski, Octupolly deformed nuclei near ^{112}Ba , *Phys. Lett. B* **238**, 6 (1990).
- [96] P.-H. Heenen, J. Skalski, P. Bonche, and H. Flocard, Octupole excitations in light xenon and barium nuclei, *Phys. Rev. C* **50**, 802 (1994).
- [97] J. Smith, C. Chiara, D. Fossan, D. LaFosse, G. Lane, J. Sears, K. Starosta, M. Devlin, F. Lerma, D. Sarantites, S. Freeman, M. Leddy, J. Durell, A. Boston, E. Paul, A. Semple, I. Lee, A. Macchiavelli, and P. Heenen, Excited states and deformation of ^{112}Xe , *Phys. Lett. B* **523**, 13 (2001).
- [98] S. L. Rugari, R. H. France, B. J. Lund, Z. Zhao, M. Gai, P. A. Butler, V. A. Holliday, A. N. James, G. D. Jones, R. J. Poynter, R. J. Tanner, K. L. Ying, and J. Simpson, Broken reflection symmetry in ^{114}Xe , *Phys. Rev. C* **48**, 2078 (1993).
- [99] L. Capponi, J. F. Smith, P. Ruotsalainen, C. Scholey, P. Rahkila, K. Auranen, L. Bianco, A. J. Boston, H. C. Boston, D. M. Cullen, X. Derkx, M. C. Drummond, T. Grahn, P. T. Greenlees, L. Grocutt, B. Hadinia, U. Jakobsson, D. T. Joss, R. Julin, S. Juutinen, M. Labiche, M. Leino, K. G. Leach, C. McPeake, K. F. Mulholland, P. Nieminen, D. O'Donnell, E. S. Paul, P. Peura, M. Sandzelius, J. Saren, B. Saygi, J. Sorri, S. Stolze, A. Thornthwaite, M. J. Taylor, and J. Uusitalo, Direct observation of the $^{114}\text{Ba} \rightarrow ^{110}\text{Xe} \rightarrow ^{106}\text{Te} \rightarrow ^{102}\text{Sn}$ triple α -decay chain using position and time correlations, *Phys. Rev. C* **94**, 024314 (2016).
- [100] J. Lippuner and L. F. Roberts, r -process lanthanide production and heating rates in kilonovae, *Astrophys. J.* **815**, 82 (2015).
- [101] S. A. Giuliani, G. Martinez-Pinedo, and L. M. Robledo, Fission properties of superheavy nuclei for r -process calculations, *Phys. Rev. C* **97**, 034323 (2018).
- [102] S. A. Giuliani, G. Martinez-Pinedo, M. R. Wu, and L. M. Robledo, Fission and the r -process nucleosynthesis of translead nuclei, [arXiv:1904.03733](https://arxiv.org/abs/1904.03733) [nucl-th].